PLL synchronization stability analysis of MMC-connected wind farms under high-impedance AC Faults

Li, Yingbiao; Wang, Xiongfei; Guo, Jianbo; Wu, Heng; Zhao, Bing; Wang, Shanshan; Wu, Guanglu; Wang, Tiezhu

Published in:
IEEE Transactions on Power Systems

DOI (link to publication from Publisher):
10.1109/TPWRS.2020.3025917

Publication date:
2021

Document Version
Accepted author manuscript, peer reviewed version

This article has been accepted for publication in a future issue of this journal, but has not been fully edited. Content may change prior to final publication. Citation information: DOI 10.1109/TPWRS.2020.3025917, IEEE Transactions on Power Systems

PLL Synchronization Stability Analysis of MMC-Connected Wind Farms under High-Impedance AC Faults

Yingbiao Li, *Member, IEEE*, Xiongfei Wang, *Senior Member, IEEE*, Jianbo Guo, *Senior Member, IEEE*, Heng Wu, *Student Member*, Bing Zhao, Shanshan Wang, Guanglu Wu, Tiezhu Wang

***Abstract*—This paper analyzes the transient stability of an offshore wind farm connected via modular multilevel converter (MMC)-based high-voltage direct-current transmission system. The wind farm is composed by full-scale type-4 wind turbines, whereas short-circuit faults occurring in between the MMC and wind farm are considered. The MMC tends to be switched to the current limiting mode or the overmodulation mode during the ac-side fault, which further interacts with the control systems of wind turbines, complicating the transient stability problem of the system. Hence, in this work the parametric impacts of the phase-locked loop of wind turbine converters and over-current/-modulation limiters of the MMC are revealed analytically, and further corroborated by time-domain simulations.**

Keywords—Modular Multilevel Converter, transient stability, wind power plant, short-circuit faults, equilibrium points

I. INTRODUCTION

Modular multilevel converter (MMC) based high-voltage direct current (HVDC) transmission systems have been increasingly deployed to interconnect offshore wind farms to the power grid [1]. In order to guarantee the reliable operation of the system, the fault ride through (FRT) capability of wind turbines is specified by grid codes [2]. As the precondition of the successful FRT, the synchronization stability (i.e. transient stability) of wind turbines under grid faults has to be assured.

The MMC is operating as an ac voltage source for the wind farm, forming the system voltage and frequency [3], [4]. In contrast, wind turbines, which are generally type-4 in offshore applications, are synchronized with the MMC via the phase-locked loop (PLL) used with their grid-side converters (GSC), and inject active and reactive power through the vector current control [5]. And the grid-side converter is based on the 2-Level Voltage-Source Converter (2L-VSC). The small-signal stability of the MMC-connected wind farms have been analyzed in [6], [7]. It is found that the PLL has a significant effect on the system stability. However, what remains unclear is the transient stability of such a system subjected to large disturbances, e.g. whether the wind farm is loss of synchronization (LOS) under the short-circuit faults in between the wind farm and MMC [8].

There have been increasing research efforts spent on the transient stability of the grid-connected converters [9]-[11]. It is found out that transient instability is more likely to happen during severe short-circuit faults in weak ac grids [11]. A necessary condition for the stable operation is the existence of equilibrium points for the PLL-synchronized converters. However, considering the second-order nonlinear dynamic of the PLL, the LOS may still arise even with equilibrium points [12]. There are mainly two approaches to investigate the transient stability, including: Lyapunov's method and phase portrait. For Lyapunov's method, a Lyapunov function is necessary to investigate the transient stability [13]. Equal Area Criterion (EAC) is a special case of Lyapunov's method. Ignoring the proportional gain of the proportional- integral (PI) controller of PLL, the LOS mechanism of grid-connected converters is analyzed with EAC in [12]. Yet, the P controller cannot be ignored in practice. As shown in [9], how to develop an appropriate Lyapunov function and how to apply it to analyze LOS of MMC-connected converters is still an unresolved challenge interior to the field of direct methods of synchronization stability for 2L-VSCs. Based on phase portrait, a design-oriented analysis approach to the transient stability of grid-connected converters is introduced in [14]-[16]. The obvious advantage of this approach is the parametric impacts of PLL and the grid impedance can be identified, and thus provides clear insight into the controller design. On the grid side, the LOS is related to the impedance of the transmission line and the voltage of the grid-connected point after faults. On the converter side, the output current and the PLL parameters can both destabilize the system [16]-[18]. To address the instability, an adaptive PLL is thus reported [16]. However, all those studies only consider the scenario that the converter is connected to an infinite bus with different line impedances. This assumption no longer holds in the MMC-connected wind farms.

Due to the limited overcurrent capability of MMC, proper current limiting control schemes are always required [19]. In the presence of severe faults at the ac side of MMC, the MMC is switched to the current limiting mode, and the MMC is equivalent to a current source [20]. Further, in the presence of high-impedance ac faults, the fault current may be within the overcurrent limit of MMC, and then the MMC can still operate as a voltage source, yet may trigger the overmodulation mode. Therefore, the MMC tends to be equivalent to a current source or a voltage source during the ac-side fault complicating the transient stability problem of the system. Furthermore,

This work is supported by State Grid Corporation of China under Technology Project No. XT71-18-007.

Yingbiao Li is with the School of Electrical and Electronic Engineering, Huazhong University of Science and Technology, 430074, Wuhan, China and was with China Electric Power Research Institute, 100192, Beijing, China.

Jianbo Guo is with China Electric Power Research Institute, 100192, Beijing, China and also with the School of Electrical and Electronic Engineering, Huazhong University of Science and Technology, 430074, Wuhan, China

Bing Zhao, Shanshan Wang, Guanglu Wu and Tiezhu Wang are with China Electric Power Research Institute, 100192, Beijing, China.

Xiongfei Wang and Heng Wu are with the Department of Energy Technology, Aalborg University 9220 Aalborg, Denmark

Corresponding Author: Xiongfei Wang, E-mail: xwa@et.aau.dk

This article has been accepted for publication in a future issue of this journal, but has not been fully edited. Content may change prior to final publication. Citation information: DOI 10.1109/TPWRS.2020.3025917, IEEE Transactions on Power Systems

different from the infinite bus, the initial phase of MMC can be controlled during the fault and has an impact on the transient stability. Hence, the high-impedance fault can lead to a more complex transient stability characteristic of the MMC-connected wind farms system. The interaction between the MMC and wind farm during ac-side faults is the focus of this work. To investigate the stability, phase portrait method is used to analyze the transient stability of power system.

This paper thus aims to investigate the transient stability of the MMC-connected wind farm under the high-impedance ac fault and the 2L-VSCs are equivalent to one converter in the paper. First, the possible operation modes of the MMC after the fault are identified. Second, the conditions for the existence of equilibrium points are analyzed in different MMC operation modes. Then, the parametric impacts of the PLL of 2L-VSC of wind turbines, and the current/modulation signal limiters of MMC on transient stability is revealed. Lastly, time-domain simulations validate the theoretical analysis.

II. Operation Modes of MMC

A. System Description

Fig. 1 (a) illustrates the single-line diagram of the MMC-connected wind turbines in the *dq* frame. To limit the fault current, a dual-loop control including the outer voltage loop control and the inner current loop control is used. Without loss of generality, the 2L-VSCs are equivalent to one converter using an aggregated model [21]. The control diagram of 2L-VSC is shown as Fig. 1 (b), where the PLL is used to detect the voltage phase at the grid-connected point, and thus synchronized the 2L-VSC with the MMC. A constant dc-link voltage of the MMC is assumed, while wind turbines are simplified as a converter with a constant DC current [6] as shown in Fig. 1 (c). The transient stability of the system under ac-side symmetrical faults, as shown in Fig. 1 (a), is studied in this work.

In Fig. 1, u_{ms} denotes the voltage at the point of common connection (PCC), u_{mc} is the output voltage of MMC, i_m is the current injected into MMC, u_{ws} is the voltage at the grid-connected point of 2L-VSC, i_w is the output current of wind turbine, Z_{eq} is the equivalent inductance of MMC, Z_{line} is the equivalent inductance of transmission line and the transformers of 2L-VSC, L_{fil} and C_{fil} are the output filter of 2L-VSC and "*" represents the reference of the current and voltage. Through decoupling control, the active power can be controlled by i_{wd} and reactive power can be controlled by i_{wq}. Therefore, i_{wd} is named active-current and i_{wq} is named reactive-current. When there is a high-impedance ac fault, the 2L-VSC can inject both active-current and reactive-current based on the grid codes [2].

B. Post-Fault Characteristics of the System

1) Equivalent Circuit

When there is no fault, the MMC can be equivalent to a voltage source and the 2L-VSC can be equivalent to a current source as shown in Fig. 2 (a). The current injected into MMC is equal to the current of 2L-VSC. However, when there is a short circuit fault, as shown in Fig. 1 (a), the equivalent circuit is changed as Fig. 2 (b), and the current flowing into the MMC will be changed. Based on the circuit, the fault current of the MMC can be calculated as

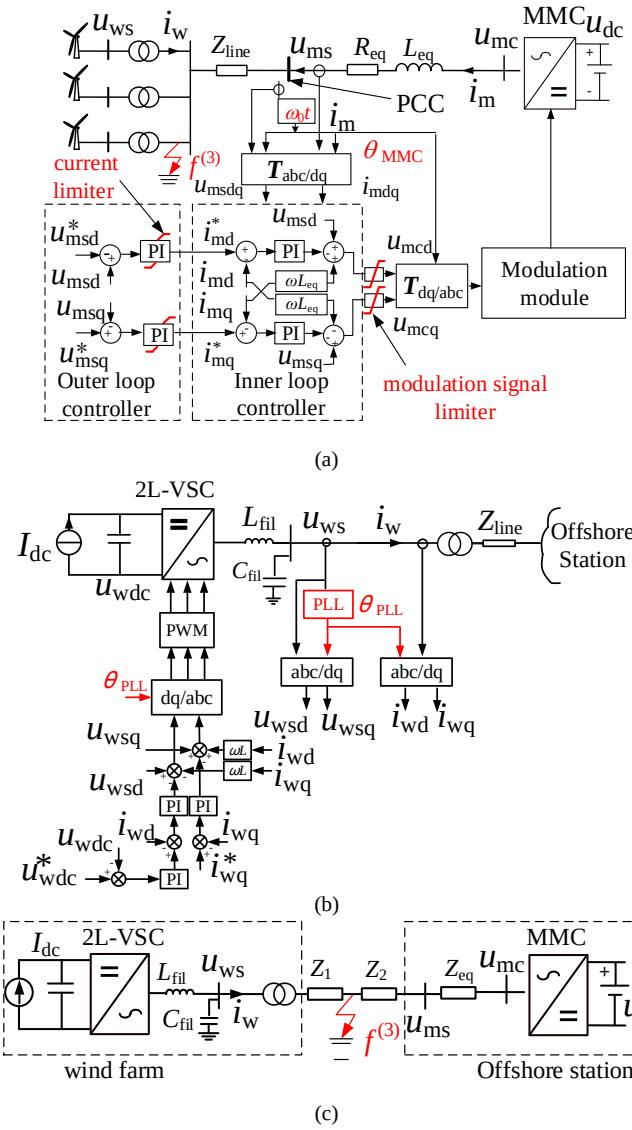

Fig. 1. Control block diagram and circuit topology. (a) Single-line diagram of MMC with dual-loop voltage control. (b) Single-line diagram of 2L-VSC of wind turbine. (c) Equivalent Circuit of the system.

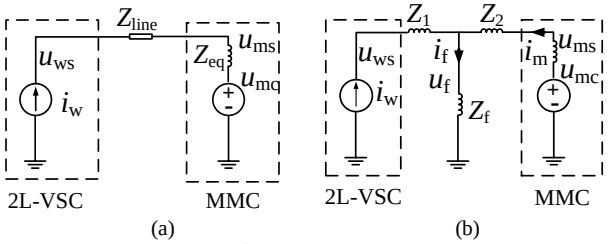

Fig. 2. Single-line diagram of the MMC-connected wind turbine system. (a) Equivalent circuit before the fault. (b) Equivalent circuit after the fault.

$$i_m = \frac{u_{mc} - i_w Z_f}{Z_2 + Z_f + Z_{eq}} \tag{1}$$

where Z_f is the impedance of the fault and the controller effect is ignored because only the characteristics of the circuit is investigated in this part.

From (1) it can be seen that the current of MMC is increased from i_w to i_m and u_{ms} is decreased when there is a fault. The value of i_m is dependent on the output voltage of MMC, the fault impedance Z_f, the fault location and the current of 2L-VSC.

2) Impacts of Controllers

This article has been accepted for publication in a future issue of this journal, but has not been fully edited. Content may change prior to final publication. Citation information: DOI 10.1109/TPWRS.2020.3025917, IEEE Transactions on Power Systems

The changes of voltage and current after the fault have an effect on the controller. The mathematical model of the outer voltage loop is obtained as

$$\begin{cases} i_{\mathrm{md}}^{*} = K_{\mathrm{pv}} \cdot (u_{\mathrm{msd}} - u_{\mathrm{msd}}^{*}) + K_{\mathrm{iv}} \cdot \int (u_{\mathrm{msd}} - u_{\mathrm{msd}}^{*}) \mathrm{d}t \\ i_{\mathrm{mq}}^{*} = K_{\mathrm{pv}} \cdot (u_{\mathrm{msq}} - u_{\mathrm{msq}}^{*}) + K_{\mathrm{iv}} \cdot \int (u_{\mathrm{msq}} - u_{\mathrm{msq}}^{*}) \mathrm{d}t \end{cases} \tag{2}$$

where K_{pv} and K_{iv} are the proportional gain and integral gain of the outer loop PI regulator.

When there is a short circuit fault, the voltage of u_{ms} is smaller than the reference value u_{ms}^{*}. The current reference generated by the outer loop regulator may reach the lower limit of the current limiter according (2). The mathematical model of the inner current loop is obtained as

$$\begin{cases} u_{\mathrm{dPI}} = K_{\mathrm{pi}} \cdot (i_{\mathrm{md}}^{*} - i_{\mathrm{md}}) + K_{\mathrm{ii}} \cdot \int (i_{\mathrm{md}}^{*} - i_{\mathrm{md}}) \mathrm{d}t \\ u_{\mathrm{qPI}} = K_{\mathrm{pi}} \cdot (i_{\mathrm{mq}}^{*} - i_{\mathrm{mq}}) + K_{\mathrm{ii}} \cdot \int (i_{\mathrm{mq}}^{*} - i_{\mathrm{mq}}) \mathrm{d}t \end{cases} \tag{3}$$

and the output voltage of MMC can be obtained as

$$\begin{cases} u_{\mathrm{mcd}} = u_{\mathrm{msd}} - u_{\mathrm{dPI}} + i_{\mathrm{mq}} \omega L_{\mathrm{eq}} \\ u_{\mathrm{mcq}} = u_{\mathrm{msq}} - u_{\mathrm{qPI}} - i_{\mathrm{md}} \omega L_{\mathrm{eq}} \end{cases} \tag{4}$$

where K_{pi} and K_{ii} are the proportional gain and integral gain of the inner PI regulator, u_{dPI} and u_{qPI} are the output value of the inner PI regulators, ω is the angular frequency.

C. Operation Modes of MMC

Focusing on the interaction between the MMC and 2L-VSC during ac-side faults, only the cases where the current or voltage triggers the limiter after the fault are investigated. Based on the fault current calculated by (1) and the effect of the controller, two operation modes can be obtained, which are elaborated as follows:

1) Current Limiting Mode

In this case, the fault current calculated by (1) violates the current limit. The PCC voltage is lower than the reference value as shown in Fig. 3 (a) and the current reference reaches the lower limit of the current limiter which is shown in Fig. 3 (b). Then there will be a positive input error into the inner current loop as shown in Fig. 3 (b). Consequently, the output voltage of MMC is reduced based on (4) as shown in Fig. 3 (a), and the fault current is limited to the limit value I_{mmax} as shown in Fig. 3 (b). The MMC is operated in current limiting mode as a current source which is shown as Fig. 4 (a).

It should be noted that, when there is a low-impedance ac faults, the Z_{f} is much smaller and the fault current calculated by (1) always violates the current limit. Therefore, the MMC can only be operated in current limiting mode as a current source under low-impedance AC faults.

2) Overmodulation Mode

In another case, the amplitude of fault current calculated by (1) is lower than the amplitude of limit value, while the current reference reaches the lower limit of the current limiter which is shown in Fig. 5 (b). Consequently, there will be a negative input error in the inner current controller, as shown in Fig. 5(b). Based on (4), the output voltage of MMC is increased, yet its maximum value is limited by the modulation signal limiter.

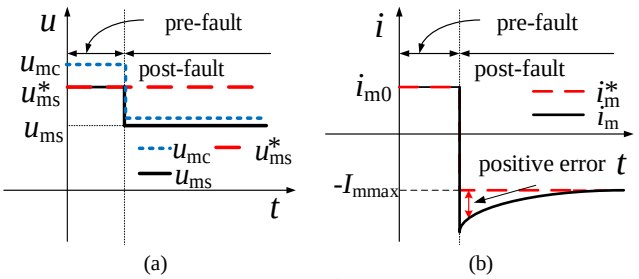

Fig. 3. Current and voltage dynamics of MMC in current limiting mode. (a) MMC voltage and voltage reference. (b) Current and current reference.

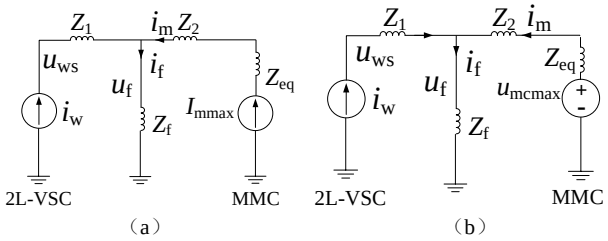

Fig. 4. Single-line diagram of the MMC-connected wind turbine system. (a) Current limiting mode of MMC. (b) Overmodulation mode of MMC.

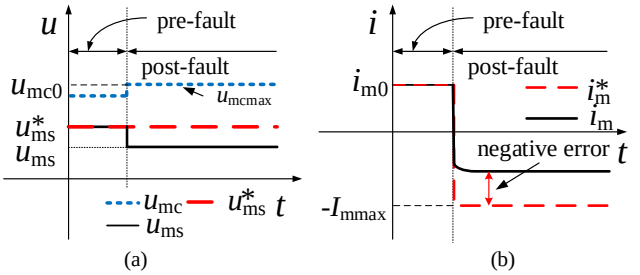

Fig. 5. Current and voltage dynamics of MMC in the overmodulation mode. (a) MMC voltage and voltage reference. (b) Current and current reference.

When the voltage of u_{mc} reaches the maximum value u_{mcmax}, as shown in Fig. 5 (a), the output voltage of MMC is saturated at the limit of modulation signal and the error between the real current and the reference current cannot be eliminated. The MMC is operated in overmodulation mode as a voltage source which is shown in Fig. 4 (b).

III. Existence of Equilibrium Points

A. Mathematical Model of PLL

The block diagram of PLL is shown in Fig. 6, where θ_{PLL} can be obtained as

$$\theta_{\mathrm{PLL}} = \int \omega_1 \mathrm{d}t \tag{5}$$

where

$$\begin{cases} \omega_1 = \Delta\omega + \omega_0 \\ \Delta\omega = K_{\mathrm{PPLL}} \cdot u_{\mathrm{wsq}} + K_{\mathrm{iPLL}} \cdot \int u_{\mathrm{wsq}} \mathrm{d}t \end{cases} \tag{6}$$

and ω_0 is the nominal grid frequency, ω_1 is output frequency of PLL, K_{pPLL} and K_{iPLL} are the proportional gain and integral gain of PI controller.

The constant frequency control is implemented in the voltage-controlled MMC. The phase of PCC voltage of MMC can be calculated as

$$\theta_{\mathrm{MMC}} = \int \omega_0 \mathrm{d}t \tag{7}$$

δ is defined as the difference between the dq frames of MMC and 2L-VSC which can be obtained as (8).

This article has been accepted for publication in a future issue of this journal, but has not been fully edited. Content may change prior to final publication. Citation information: DOI 10.1109/TPWRS.2020.3025917, IEEE Transactions on Power Systems

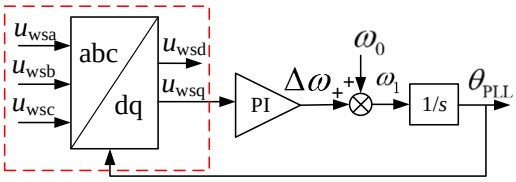

Fig. 6. Block diagram of PLL.

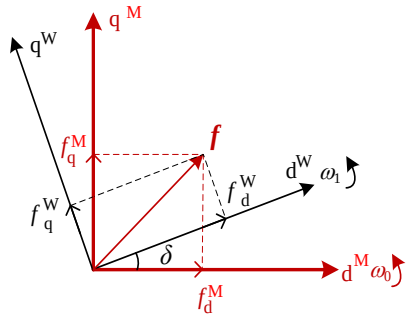

Fig. 7. Angle difference between the frames of 2L-VSC and MMC.

$$\delta = \theta_{PLL} - \theta_{MMC} = \int \left(K_{PPLL} \cdot u_{wsq} + K_{PPLL} \cdot \int u_{wsq} \mathrm{d}t \right) \mathrm{d}t \tag{8}$$

which can be regarded as the power angle between MMC and 2L-VSC. The synchronous stability can be analyzed based on the dynamic of δ.

As shown in Fig. 7, the mark "M" represents the *dq* frame of MMC and "W" represents the *dq* frame of 2L-VSC. According to Fig. 7, the relationship between the two frames can be seen as

$$\begin{cases} f_d^W = f_d^M \cos\delta + f_q^M \sin\delta \\ f_q^W = f_q^M \cos\delta - f_d^M \sin\delta \end{cases} \tag{9}$$

where f can be either the voltage or current.

B. Existence of Equilibrium Points

1) Current Limiting Mode

When the MMC is operated in current limiting mode, the equivalent circuit is shown in Fig. 4 (a), from which, u_{wsq} can be calculated as

$$u_{wsq} = \omega_1 L_f i_{md} + \omega_1 L_f i_{wd} + \omega_1 L_1 i_{wd} \tag{10}$$

where the parasitic resistance is ignored and ω_1 is output frequency of PLL.

Based on (9), in the *dq* frame of 2L-VSC, u_{wsq} can be derived as

$$u_{wsq} = \omega_1 L_f I_{mmax} \sin(\delta + \varphi_0) + \omega_1 (L_f + L_1) i_{wd} \tag{11}$$

where

$$\begin{cases} \varphi_0 = \arctan \dfrac{I_{d\_lim}^M}{I_{q\_lim}^M} + n \cdot \pi \\ I_{mmax} = \sqrt{(I_{d\_lim}^M)^2 + (I_{q\_lim}^M)^2} \end{cases} \tag{12}$$

$I_{d\_lim}^M$ and $I_{q\_lim}^M$ are the current limit values of *d*-axis and *q*-axis in *dq* frame of MMC, I_{mmax} is the maximum output current of MMC, n is an integer.

From Fig. 6, the condition for the existence of equilibrium points of PLL can be defined as $u_{wsq} = 0$ [16], which leads to

$$\omega_1 L_f I_{mmax} \sin(\delta + \varphi_0) + \omega_1 (L_f + L_1) i_{wd} = 0 \tag{13}$$

The existence of the solution of (13) requires

$$(L_f + L_1) i_{wd} = -L_f I_{mmax} \sin(\delta + \varphi_0) \le L_f I_{mmax} \tag{14}$$

which indicates that the existence of equilibrium points is affected by both the injected *d*-axis current of 2L-VSC and the maximum output current of MMC. In order to avoid the LOS, (14) needs to be satisfied.

2) Overmodulation Mode

When the MMC is operated in overmodulation mode, the equivalent circuit is shown in Fig. 4 (b), based on which, the u_{wsq} can be calculated as

$$u_{wsq} = \frac{K \cdot i_{wd} + u_{mcq} L_f}{(L_2^* + L_f)} \tag{15}$$

where

$$\begin{cases} L_2^* = L_2 + L_{eq} \\ K = \omega_1 (L_1 L_2^* + L_2^* L_f + L_1 L_f) \end{cases} \tag{16}$$

and the resistance is ignored.

Then, based on (9), u_{wsq} can be derived in the *dq* frame of 2L-VSC, which is given by

$$u_{wsq} = \frac{K \cdot i_{wd} - u_{mcmax} \sin(\delta - \varphi_1) L_f}{(L_2^* + L_f)} \tag{17}$$

where

$$\begin{cases} \varphi_1 = \arctan \dfrac{u_{mcq\_lim}^M}{u_{mcd\_lim}^M} + n \cdot \pi \\ u_{mcmax} = \sqrt{(u_{mcq\_lim}^M)^2 + (u_{mcd\_lim}^M)^2} \end{cases} \tag{18}$$

$u_{mcd\_lim}^M$ and $u_{mcq\_lim}^M$ are the modulation signal limit values of *d*- and *q*-axis in *dq* frame of MMC. u_{mcmax} is the maximum output voltage of MMC.

Considering the condition for the existence of equilibrium points of PLL, i.e. u_{wsq}=0, which leads to

$$K \cdot i_{wd} - u_{mcmax} \sin(\delta - \varphi_1) L_f = 0 \tag{19}$$

The existence of the solution of (19) requires

$$K \cdot i_{wd} = L_f u_{mcmax} \sin(\delta - \varphi_1) \le L_f u_{mcmax} \tag{20}$$

It is known from (20) that the existence of equilibrium points is affected by the injected *d*-axis current of 2L-VSC and the maximum output voltage of MMC. The LOS will be inevitable if (20) is not satisfied.

IV. TRANSIENT STABILITY ANALYSIS

When there are no equilibrium points, the LOS is inevitable. However, when there are equilibrium points, the LOS can also arise [16]. In this section, the transient stability is analyzed by using the phase portrait approach.

A. Transient Stability Analysis in Current Limiting Mode

When the MMC is operated in current limiting mode, based on (11), the u_{wsq} can be calculated as

$$\begin{aligned} u_{wsq} &= \omega_1 (L_f + L_1) i_{wd} - \omega_1 \left[L_f I_{mmax} \sin(-\delta - \varphi_0) \right] \\ &= \omega_1 (F_1 - F_2) \end{aligned} \tag{21}$$

where

This article has been accepted for publication in a future issue of this journal, but has not been fully edited. Content may change prior to final publication. Citation information: DOI 10.1109/TPWRS.2020.3025917, IEEE Transactions on Power Systems

$$\begin{cases} F_1 = (L_f + L_1) i_{wd} \\ F_2 = L_f I_{mmax} \sin(-\delta - \varphi_0) \end{cases} \tag{22}$$

The curves of the two functions are expressed in the same frame. By comparing the size of F_1 and F_2, the value of u_{wsq} can be judged as shown in Fig.8 where δ_0 is the initial angle. It can be clearly seen from Fig.8 that $F_1 < F_2$ above the red dotted line and $u_{wsq} < 0$. Below the red dotted line, $F_1 > F_2$ and $u_{wsq} > 0$.

From Point a to Point b, $u_{wsq} > 0$ and $\Delta\omega > 0$ result in the output frequency of 2L-VSC higher than ω_0 based on (6), and thus δ is increased. When it reaches Point b, where $u_{wsq} = 0$, considering the integrator of PLL, $\Delta\omega$ is still larger than 0. From Point b to Point c, $u_{wsq} < 0$ and $\Delta\omega$ starts to decrease. When $\Delta\omega = 0$, δ will not be increased anymore and begins returning to Point b. It is noted that $u_{wsq} > 0$ when the operation point exceeds Point c. If $\Delta\omega$ is still higher than 0 at Point c, then $\Delta\omega$ will always be higher than 0 and δ will continue to be increased, leading to the LOS. Therefore, Point b is a stable point while Point c is an unstable point [16].

Substituting (11) into (8), considering the relationship of $X_L = (\dot{\delta} + \omega_0)L$, the phase portrait of PLL can be obtained as (24) in the bottom of this page, which can describe the dynamic of δ. From (24), it can be seen that the transient stability is affected by the parameters K_{pPLL} ,K_{iPLL}, i_{wd}, I_{mmax}, and φ_0.

1) Parametric Effect of PLL

Generally, the PLL is characterized by two important parameters, i.e. damping ratio (ζ) and settling time (t_s), which can be expressed by the controller parameters of the PLL as

$$\begin{cases} \xi = \dfrac{K_{pPLL}}{2}\sqrt{\dfrac{V_{gn}}{K_{iPLL}}} \\ t_s = \dfrac{9.2}{V_{gn} K_{pPLL}} \end{cases} \tag{23}$$

where V_{gn} is the nominal grid voltage.

Substituting (23) into (24), the parametric effect of PLL can be obtained. Under the condition of $I_{mmax} = 6$ kA, $i_{wd} = 0.13$p.u., $\varphi_0 = 0.5\,\pi$, the phase portraits are shown in Fig. 9. In Fig. 9 (a), $t_s = 0.3$, when $\zeta = 0.5$ or 0.3, the operating point is converged to Point b, which is the stable equilibrium point (SEP) from the initial Point a. But the phase portrait is diverged when $\zeta = 0.1$ which means the 2L-VSC and MMC are asynchronous. In Fig. 9 (b) , the effect of t_s on the stability is revealed when $\zeta = 0.2$. It can be seen that the synchronization stability is guaranteed when $t_s = 0.2$ or 0.1. On the contrary, the system is unstable when $t_s = 0.02$. Therefore, the transient stability of the system can be enhanced by increasing damping ratio and settling time of PLL of 2L-VSC.

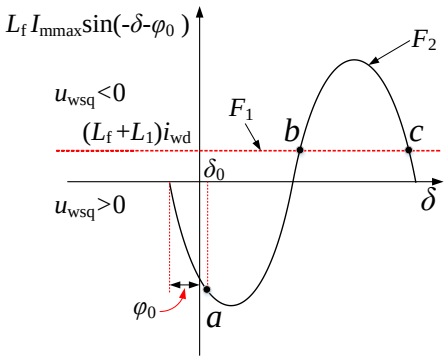

Fig. 8. Current-angle curve of MMC-connected 2L-VSC in the Current Limiting Mode.

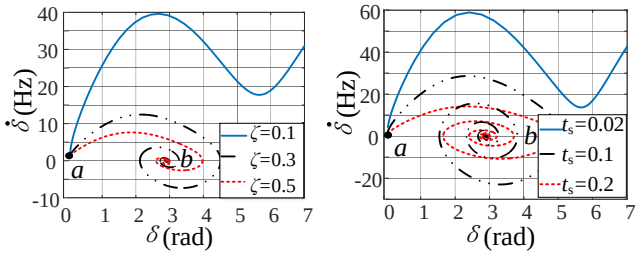

(a) (b)

Fig. 9. Phase portraits of PLL in current limiting mode, $I_{mmax} = 6$ kA, $i_{wd} = 0.13$ p.u., $\varphi_0 = 0.5\,\pi$. (a) $t_s = 0.3$, $\zeta = 0.5$ (stable), $\zeta = 0.3$ (stable), $\zeta = 0.1$ (unstable). (b) $\zeta = 0.2$, $t_s = 0.2$ (stable), $t_s = 0.1$ (stable), $t_s = 0.02$ (unstable).

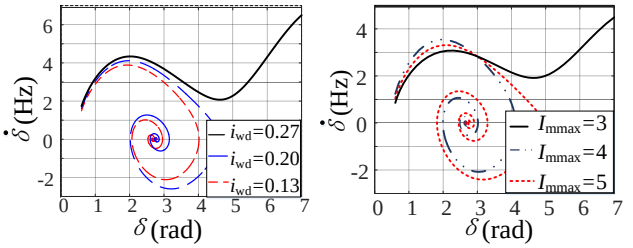

(a) (b)

Fig. 10. Phase portraits of PLL in current limiting mode ,$t_s = 0.3$, $\zeta = 0.5$, $\varphi_0 = 0.5\,\pi$. (a) $I_{mmax} = 6$ kA, $i_{wd} = 0.27$ p.u. (unstable), $i_{wd} = 0.2$ p.u. (stable), $i_{wd} = 0.13$ p.u. (stable). (b) $i_{wd} = 0.13$ p.u., $I_{mmax} = 5$ kA (stable), $I_{mmax} = 4$ kA (stable), $I_{mmax} = 3$ kA (unstable).

2) Effects of 2L-VSC Current and MMC Current

The effects of i_{wd} and I_{mmax} on the transient stability are illustrated in Fig. 10, considering that $t_s = 0.3$, $\zeta = 0.5$, $\varphi_0 = 0.5\,\pi$. Fig. 10 (a) shows the phase portraits with different i_{wd} and Fig. 10 (b) shows the phase portraits with different I_{mmax}. It is clear that the system is stable when the phase portrait converges, as shown by the dashed lines, and is unstable when the phase portrait diverges, as shown by solid lines. Therefore, the synchronization stability can be enhanced by reducing i_{wd} and increasing I_{mmax} which means increasing the regulation range from Point b to Point c in Fig.8.

$$\ddot{\delta} = \frac{\left[\begin{array}{c} \left(K_{pPLL} L_f I_{mmax} \omega_0 \cos(\delta+\varphi_0) + K_{iPLL} L_f I_{mmax} \sin(\delta+\varphi_0) + K_{iPLL}(L_f + L_1) i_{wd}\right)\dot{\delta} + \\ K_{pPLL} \cos\delta L_f I_{mmax} \left(\dot{\delta}\right)^2 + K_{iPLL}\omega_0 \left(L_f I_{mmax} \sin(\delta+\varphi_0) + (L_f + L_1) i_{wd}\right) \end{array}\right]}{1 - K_{pPLL}\left(L_f I_{mmax} \sin(\delta+\varphi_0) + (L_f + L_1) i_{wd}\right)} \tag{24}$$

This article has been accepted for publication in a future issue of this journal, but has not been fully edited. Content may change prior to final publication. Citation information: DOI 10.1109/TPWRS.2020.3025917, IEEE Transactions on Power Systems

3) Effect of φ_0.

φ_0 has an effect on the initial phase of the current of MMC and is affected by the current limit value in *d*- and *q*-axis during the fault as (12). In order to ensure that the δ can be converged to Point b, the length from Point a to b should be shortened and the length from Point b to Point c should be increased, as shown in Fig.8, which can be realized by controlling φ_0 based on (12). From Fig. 11 (a) and (b) it can be seen that the length from Point a to Point b is shortened when $\varphi_0 > 0$ and increased when $\varphi_0 < 0$. Therefore, φ_0 should be set as higher than 0. Furthermore, δ_0 is always in the range between 0 and $\pi/2$. Since the Point c is an unstable point, to ensure that the initial Point a doesn't exceed Point c, the condition needs to be met as (25).

$$\delta_0 + \varphi_0 < 1.5\pi \tag{25}$$

Consequently, $\varphi_0 \leq \pi$ should be required. Otherwise, the system becomes unstable, as shown in Fig. 11 (d), when $\varphi_0 = 1.5\,\pi$. Under the condition that $t_s = 0.3$, $\zeta = 0.5$, $I_{mmax} = 6$ kA, $i_{wd} = 0.13$ p.u., phase portraits are shown in Fig. 12 and it can be seen that the transient stability is enhanced when $\varphi_0 = \pi$.

Therefore, φ_0 should be set as π during the fault shown in Fig. 11 (c), which leads to

$$\begin{cases} I_{\mathrm{d\_lim}}^{\mathrm{M}} = 0 \\ I_{\mathrm{q\_lim}}^{\mathrm{M}} = -I_{\mathrm{mamx}} \end{cases} \tag{26}$$

B. Transient Stability Analysis in Overmodulation mode

When MMC is operated in overmodulation mode, based on (17), the voltage-angle curve of 2L-VSC is shown as Fig. 13, where δ_0 is initial angle. Substituting (17) into (8), the phase portrait of PLL can be obtained as (27) in the bottom of this page, which can describe the dynamic of δ. From (27), it can be seen that the transient stability is affected by the parameters K_{pPLL} ,K_{iPLL}, i_{wd}, u_{mcmax}, and φ_1.

1) Parametric Effect of PLL

Considering that $u_{cmax} = 1.3$ p.u., $i_{wd} = 0.4$ p.u., $\varphi_1 = 1.57$ rad, the effect of ζ and t_s on transient stability are revealed as Fig. 14. It is clear that the system is stable when the phase portrait converges, as shown by the dashed lines, and is unstable when the phase portrait diverges, as shown by solid lines. Therefore, the transient stability is enhanced by increasing ζ and t_s.

2) Impacts of 2L-VSC Current and MMC Voltage

The effect of i_{wd} and u_{mcmax} on stability are shown in Fig. 15 under the condition of $t_s = 0.3$, $\zeta = 0.2$, $\varphi_1 = 1.57$ rad. Fig. 15 (a) shows the phase portraits with different i_{wd} and Fig. 15 (b) shows the phase portraits with different u_{mcmax}. From Fig. 15, it can be seen that the transient stability is enhanced by reducing i_{wd} and increasing u_{mcmax} which means enlarging the regulation range from Point b to Point c in Fig. 13.

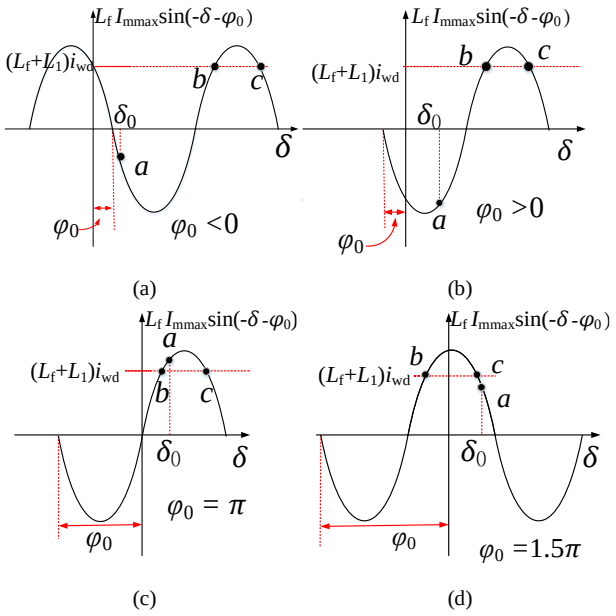

Fig. 11. Current-angle curves of MMC-connected 2L-VSC in the current limiting mode. (a) $\varphi_0 < 0$. (b) $\varphi_0 > 0$. (c) $\varphi_0 = \pi$. (d) $\varphi_0 = 1.5\,\pi$.

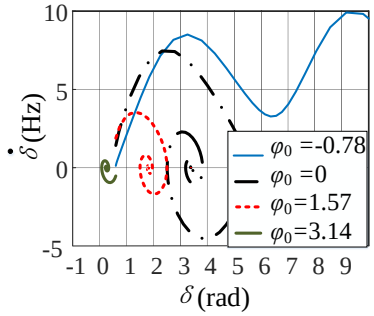

Fig. 12. Phase portraits in different φ_0, $t_s = 0.3$, $\zeta = 0.5$, $I_{mmax} = 6$ kA, $i_{wd} = 0.13$ p.u., $\varphi_0 = -0.78$ rad (unstable), $\varphi_0 = 0$ rad (stable), $\varphi_0 = 1.57$ rad (stable), $\varphi_0 = 3.14$ rad (stable).

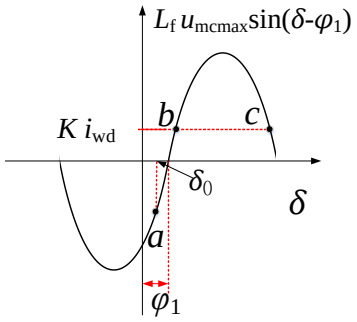

Fig. 13. Voltage-angle curve of MMC-connected 2L-VSC in the overmodulation mode.

3) Effect of φ_1.

φ_1 has an effect on the initial phase of the output voltage of MMC and is affected by the modulation signal limit values in *d*-axis and *q*-axis during the fault as (18). Also, the range of δ_0 is from 0 to $\pi/2$. To ensure that the initial Point a doesn't

$$\ddot{\delta} = \frac{\left[\begin{array}{c}\left(-K_{pPLL}u_{mcmax}L_f\cos(\delta-\varphi_1)+K_{iPLL}\left(L_1L_2^*+L_2^*L_f+L_1L_f\right)i_{wd}\right)\dot{\delta}-K_{iPLL}u_{mcmax}\sin(\delta-\varphi_1)L_f \\ +K_{iPLL}\omega_0\left(L_1L_2^*+L_2^*L_f+L_1L_f\right)i_{Wd}\end{array}\right]}{\left(L_2^*+L_f\right)-K_{pPLL}\left(L_1L_2^*+L_2^*L_f+L_1L_f\right)i_{Wd}} \tag{27}$$

This article has been accepted for publication in a future issue of this journal, but has not been fully edited. Content may change prior to final publication. Citation information: DOI 10.1109/TPWRS.2020.3025917, IEEE Transactions on Power Systems

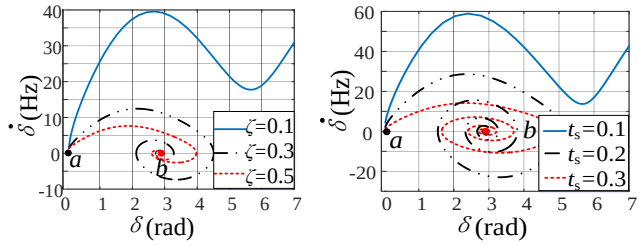

(a) (b)

Fig. 14. Phase portraits of δ in overmodulation mode, u_{cmax} = 1.3 p.u., i_{wd} = 0.4 p.u., φ_1 = 1.57 rad. (a) t_s = 0.2, ζ = 0.5 (stable), ζ = 0.3 (stable), ζ = 0.1 (unstable). (b) ζ = 0.2, t_s = 0.3 (stable), t_s = 0.2 (stable), t_s = 0.1 (unstable).

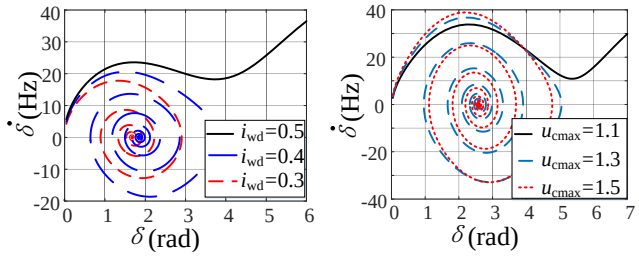

(a) (b)

Fig. 15. Phase portraits of δ in overmodulation mode, t_s = 0.3, ζ = 0.2, φ_1 = 1.57 rad. (a) u_{cmax} =1.3 p.u., i_{wd} = 0.5 p.u. (unstable), i_{wd} = 0.4 p.u. (stable), i_{wd} = 0.3 p.u. (stable). (b) i_{wd} = 0.4 p.u., u_{mcmax} =1.1 p.u. (unstable), u_{mcmax} = 1.3 p.u. (stable), u_{mcmax} = 1.5 p.u. (stable).

exceed Point c, the condition needs to be met as

$$\delta_0 - \varphi_1 < \pi/2 \tag{28}$$

Therefore, $\varphi_1 \geq 0$ should be required. As shown in Fig. 16 (a), when $\varphi_1 < 0$, the initial Point a may exceed Point c and the system becomes unstable. When $\varphi_1 > 0$, the length from Point a to Point b is increased as shown in Fig. 16 (b), which has a negative impact on transient stability. The phase portraits are shown in Fig. 17 and it can be seen that the transient stability is enhanced when φ_1=0. So the φ_1 should be set as 0 during the fault, which leads to

$$\begin{cases} u^{M}_{mcd\_lim} = u_{mcmax} \\ u^{M}_{mcq\_lim} = 0 \end{cases} \tag{29}$$

V. SIMULATIONS

To validate the theoretical analysis, time-domain simulations are carried out in the PSCAD. The MMC and 2L-VSC are equivalent to Thévenin's equivalent model 0 and the 2L-VSCs are equivalent to one convertor using an aggregated model. A constant dc-link voltage of the MMC and a constant dc current of 2L-VSC are assumed as shown in Fig. 1 (c). The parameters are given in Table I. The output frequency of PLL of 2L-VSC is limited from 45 Hz to 55 Hz.

In the first case, i_{wd} = 0.3 p.u., L_f = 0.04 H, L_1 = 0.08 H and L_2 = 0.02 H are set, as shown in Fig. 4, under the condition of $\varphi_0 = 0.5\ \pi$. According to (1), the fault current calculated is higher than 1.1 p.u., so the MMC is operated in current limiting mode. From Fig. 18 (a) and Fig. 19 (a) it can be seen that the output current of MMC is limited to 1.1 p.u. during the fault. When t_s = 0.5, ζ = 0.1 are set, the simulation results are shown in Fig. 18 and the LOS arises. It can be seen that the voltage of MMC is unstable, the frequency of 2L-VSC reaches 55 Hz, and the δ continues to be increased. When ζ = 1, under the same condition, the 2L-VSC can be synchronized

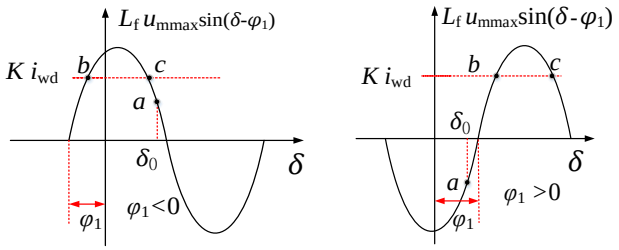

(a) (b)

Fig. 16. Voltage-angle curves of MMC-connected 2L-VSC in the overmodulation mode. (a) $\varphi_1 < 0$, Point a exceeds Point c. (b) $\varphi_1 > 0$, length from Point a to Point b is increased.

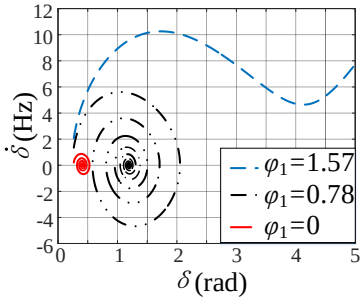

Fig. 17. Phase portraits in different φ_1, t_s = 0.3, ζ = 0.2, i_{wd} = 0.4 p.u., u_{mcmax} = 1.3 p.u., φ_1 = 0 rad (stable), φ_1 = 0.78 rad (stable), φ_1 = 1.57 rad (unstable).

TABLE I
MAIN CIRCUIT PARAMETERS USED IN SIMULATIONS

SYMBOL	DESCRIPTION	VALUE
u_{ms}	Rated ac voltage of MMC	230 kV
u_{mcmax}	The maximum value of output voltage of MMC	1.2 p.u.
u_{dc}	DC voltage of MMC	±500kV
P_m	Rated power of the MMC	1500 MW
I_{mmax}	The limit value of current limiter	1.1 p.u.
u_{ws}	Rated ac voltage of wind turbine	0.69 kV
P_w	Rated power of the wind turbine	1500 MW
L_{eq}	Equivalent inductance of MMC	0.16 p.u.
f_0	Rated frequency	50 Hz

with MMC and the system is stable as shown in Fig. 19. Comparing Fig. 18 and Fig. 19 , it can be seen that increasing ζ can enhance the transient stability of the system.

To verify the effect of t_s on transient stability, the simulations are carried out under the condition of ζ = 1. From Fig. 20 (a) it can be seen that 2L-VSC is synchronized with MMC when t_s = 0.2 and asynchronous when t_s = 0.02. The effect of t_s on transient stability is validated and transient stability can be enhanced by increasing t_s. The effect of i_{wd} on transient stability is simulated under the condition of ζ = 1, t_s = 0.2 and the results are shown as Fig. 20 (b). When i_{wd} = 0.3 p.u., the 2L-VSC is synchronized with MMC and asynchronous when i_{wd} = 0.45 p.u. which clearly demonstrates that the transient stability can be enhanced by reducing i_{wd}.

To validate the effect of φ_0, four different distribution methods of *d*-axis and *q*-axis currents of MMC during the fault are simulated, as shown in Fig. 20 (c), under the condition ζ = 0.5, t_s = 0.5. When i_{md} = -1.1 p.u. and i_{mq} = 0 p.u. (i.e. φ_0 = -π/2) are set, the power angle continues to be increased which means the LOS. When $\varphi_0 > 0$ is set, the 2L-VSC can be synchronized with MMC, and the stability is enhanced when i_{md} = 0 and i_{mq} = -1.1 p.u. (i.e. $\varphi_0 = \pi$). The calculation results based on (24) are shown as Fig. 20 (d). Comparing Fig. 20 (c) and (d), it can be seen that the equilibrium points in simulations are the same with calculation results which verifies the correctness of the theoretical analysis.

This article has been accepted for publication in a future issue of this journal, but has not been fully edited. Content may change prior to final publication. Citation information: DOI 10.1109/TPWRS.2020.3025917, IEEE Transactions on Power Systems

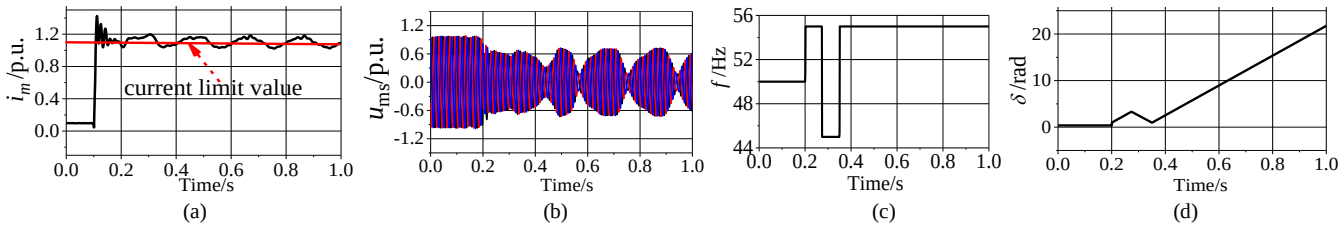

Fig. 18. Simulation results when MMC works in current limiting mode ,i_{wd}=0.3 p.u., t_s= 0.5, φ_0 = 0.5π, ζ = 0.1 ,unstable. (a) Output current of MMC. (b) Output voltage of MMC. (c) Output frequency of 2L-VSC. (d) Power angle between 2L-VSC and MMC.

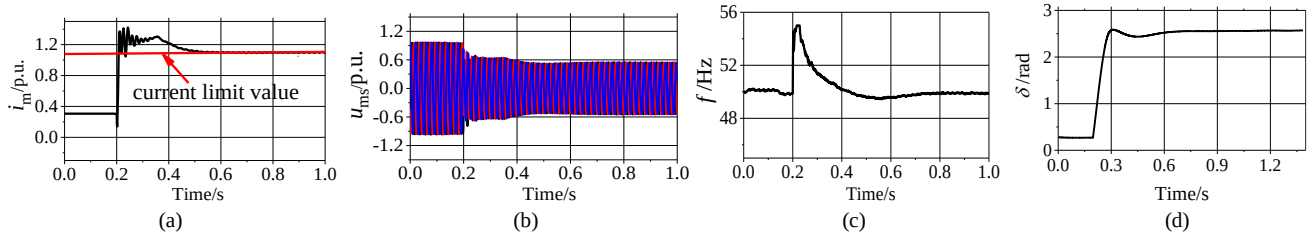

Fig. 19. Simulation results when MMC works in current limiting mode, i_{wd} = 0.3 p.u., t_s = 0.5, φ_0 = 0.5π, ζ = 1 ,stable. (a) Output current of MMC. (b) Output voltage of MMC. (c) Output frequency of 2L-VSC. (d) Power angle between 2L-VSC and MMC.

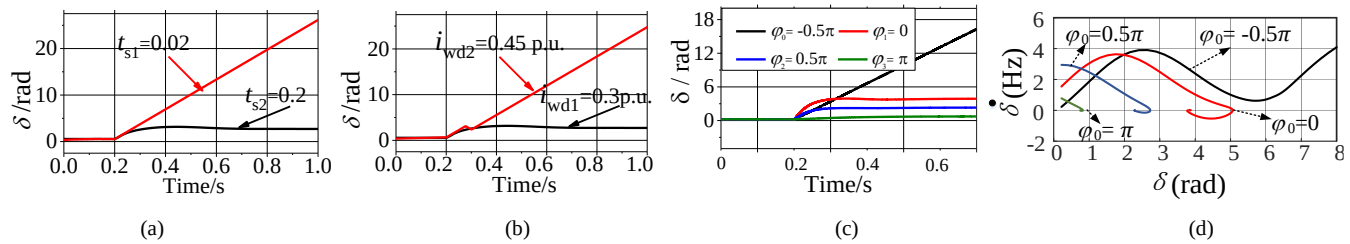

Fig. 20. Simulation results when MMC works in current limiting mode. (a) ζ = 1, i_{wd} = 0.3 p.u., t_s = 0.2 (stable), t_s = 0.02 (unstable). (b) ζ = 1, t_s = 0.2 i_{wd} = 0.3 p.u. (stable), i_{wd} = 0.45 p.u. (unstable). (c) Simulation curves of power angle with different φ_0 in Pscad. (d) Calculation curves of power angle with different φ_0 in MATLAB.

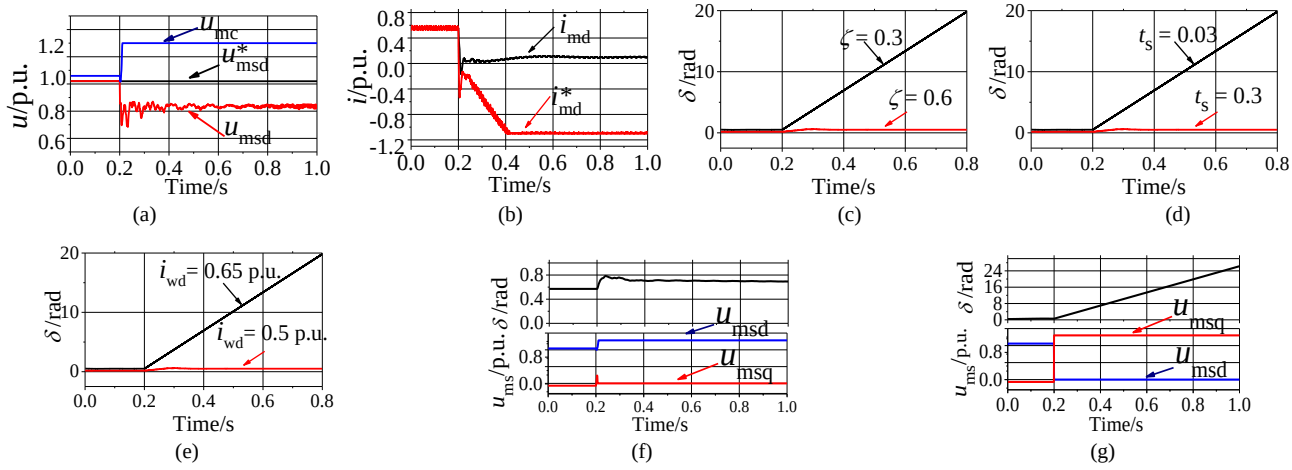

Fig. 21. Simulation results when MMC works in Overmodulation mode, φ_1 = 0, i_{wd} = 0.65 p.u.. (a) Voltage curves of MMC. (b) Current curves of MMC. (c) Power angle, t_s = 0.3, ζ = 0.6 (stable), ζ = 0.3 (unstable). (d) Power angle, ζ = 0.6, t_s = 0.3 (stable), t_s = 0.03 (unstable). (e) Power angle, ζ = 0.3, t_s =0.3, i_{wd} = 0.65 p.u. (unstable), i_{wd} = 0.5 p.u. (stable). (f) ζ =0.45, t_s = 0.2, φ_1 = 0 (stable). (g) ζ = 0.45, t_s =0.2, φ_1 = π/2, (unstable).

In the second case, i_{wd} = 0.65 p.u., L_f = 0.04 H, L_1 = 0.02 H and L_2 = 0.08 H are set. According to (1), the fault current calculated is lower than 1.1 p.u., so the MMC is operated in overmodulation mode. u_{msd} is smaller than reference value during the fault as shown in Fig. 21 (a). The current reference reaches the lower limit and there is an error between i^*_{md} and i_{md} as shown in Fig. 21 (b). It results in the output voltage of MMC reaching the higher limit as shown in Fig. 21 (a) and theMMC is operated in overmodulation mode. The parametric impact of PLL on transient stability is simulated and shown in Fig. 21 (c) and (d) under the condition of φ_1 = 0, i_{wd} = 0.65 p.u.. From Fig. 21 (c) and (d) it can be seen that the transient stability can be enhanced by increasing ζ and t_s. The effect of i_{wd} on transient stability is simulated under the condition of ζ = 0.3, t_s = 0.3 and the results are shown in Fig. 21 (e). It can be seen that decreasing i_{wd} can enhance the transient stability. The effect of initial phase φ_1 on transient stability is simulated under the condition of ζ =0.45, t_s = 0.2. The *d*-axis and *q*-axis voltage are set as u_{msd} = 1.2 p.u. and u_{msq} = 0 (i.e. φ_1 = 0) shown in Fig. 21 (f), while u_{msd} = 0 and u_{msq} = 1.2 p.u. (i.e.φ_1 = π/2) are set shown in Fig. 21 (g) during the fault. It can be seen that the 2L-VSC is synchronized with MMC when φ_1 = 0 and the LOS arises when φ_1 = π/2. Therefore, the correctness of the theoretical analysis is verified when MMC is operated in

overmodulation mode.

VI. CONCLUSIONS

This paper discusses the transient stability of MMC-connected wind turbine under the high-impedance faults. The MMC may switch to the current limiting mode or overmodulation mode depending on the fault location, fault impedance and current limit value of MMC. In different operation modes of MMC, the conditions of presence of equilibrium points are different. If there is no equilibrium point, LOS is inevitable during the fault. When there is equilibrium point, the transient stability impact of distribution of current and modulation signal limit values in *d* and *q* axes of the MMC and parameters of the PLL are revealed.

REFERENCES

[1] R. Vidal-Albalate, H. Beltran, A. Rolán, E. Belenguer, R. Peña and R. Blasco-Gimenez, "Analysis of the Performance of MMC Under Fault Conditions in HVDC-Based Offshore Wind Farms," *IEEE Trans. Power Deliv.*, vol. 31, no. 2, pp. 839-847, April 2016.

[2] BDEW Technical Guideline, Generating Plants Connected to the Medium- Voltage Network [EB/OL], June 2008 issue

[3] Y. Li, J. Guo, X. Zhang, S. Wang, S. Ma, B. Zhao, G. Wu and T. Wang, "Over-Voltage Suppression Methods for the MMC-VSC-HVDC Wind Farm Integration System," *IEEE Trans. Circuits Syst. II-Express Briefs*, vol. 67, no. 2, pp. 355-359, Feb. 2020.

[4] H. Liu and Z. Chen, "Contribution of VSC-HVDC to Frequency Regulation of Power Systems With Offshore Wind Generation," *IEEE Trans. Energy Convers.*, vol. 30, no. 3, pp. 918-926, Sept. 2015.

[5] W. Du, W. Dong and H. Wang, "Small-signal Stability Limit of a Grid-connected PMSG Wind Farm Dominated by the Dynamics of PLLs," *IEEE Trans. Power Syst.*. early access, 2019.

[6] Y. Wang, C. Zhao, C. Guo and A. U. Rehman, "Dynamic modeling and small signal stability analysis of PMSG-based wind farm with MMC-HVDC system," *CSEE J. Power Energy Syst.*. doi: 10.17775/CSEEJPES.2019.02550.

[7] H. Liu and J. Sun, "Voltage Stability and Control of Offshore Wind Farms With AC Collection and HVDC Transmission," *IEEE J. Emerg. Sel. Top. Power Electron.*, vol. 2, no. 4, pp. 1181-1189, Dec. 2014.

[8] Joint NERC and WECC Staff Report, "900 MW fault induced solar photovoltaic resource interruption disturbance report," Atlanta, USA, Feb. 2018, [Online]. Available: www.nerc.com.

[9] M. G. Taul, X. Wang, P. Davari and F. Blaabjerg, "An Overview of Assessment Methods for Synchronization Stability of Grid-Connected Converters Under Severe Symmetrical Grid Faults," *IEEE Trans. Power Electron.*, vol. 34, no. 10, pp. 9655-9670, Oct. 2019.

[10] L. Hadjidemetriou, E. Kyriakides and F. Blaabjerg, "An Adaptive Tuning Mechanism for Phase-Locked Loop Algorithms for Faster Time Performance of Interconnected Renewable Energy Sources," *IEEE Trans. Ind. Appl.*, vol. 51, no. 2, pp. 1792-1804, March-April 2015.

[11] D. Dong, B. Wen, D. Boroyevich, P. Mattavelli and Y. Xue, "Analysis of Phase-Locked Loop Low-Frequency Stability in Three-Phase Grid-Connected Power Converters Considering Impedance Interactions," *IEEE Trans. Ind. Electron.*, vol. 62, no. 1, pp. 310-321, Jan. 2015.

[12] C. Zhang, X. Cai, and Z. Li, "Transient stability analysis of wind turbines with full-scale voltage source converter," *CSEE J. Power Energy Syst.*, vol. 37, no. 14, pp. 4018–4026, July. 2017.

[13] J. Willems, "Direct method for transient stability studies in power system analysis," IEEE Trans. Autom. Control, vol. 16, no. 4, pp. 332–341, Aug. 1971.

[14] H. Wu and X. Wang, "An Adaptive Phase-Locked Loop for the Transient Stability Enhancement of Grid-Connected Voltage Source Converters," *2018 IEEE Energy Conversion Congress and Exposition (ECCE)*, Portland, OR, 2018, pp. 5892-5898.

[15] M. Taul, X. Wang, P. Davari, and F. Blaabjerg, "An efficient reduced-order model for studying synchronization stability of grid-following converters during grid faults", *Proc. IEEE COMPEL*, June 2019, in Press.

[16] H. Wu and X. Wang, "Design-Oriented Transient Stability Analysis of PLL-Synchronized Voltage-Source Converters," *IEEE Trans. Power Electron.*, early access, 2019.

[17] S. Ma, H. Geng, L. Liu, G. Yang and B. C. Pal, "Grid-Synchronization Stability Improvement of Large Scale Wind Farm During Severe Grid Fault," *IEEE Trans. Power Syst.*, vol. 33, no. 1, pp. 216-226, Jan. 2018.

[18] Ö. Göksu, R. Teodorescu, C. L. Bak, F. Iov and P. C. Kjær, "Instability of Wind Turbine Converters During Current Injection to Low Voltage Grid Faults and PLL Frequency Based Stability Solution," *IEEE Trans. Power Syst.*, vol. 29, no. 4, pp. 1683-1691, July 2014.

[19] U. Karaagac, J. Mahseredjian, L. Cai and H. Saad, "Offshore Wind Farm Modeling Accuracy and Efficiency in MMC-Based Multiterminal HVDC Connection," *IEEE Trans. Power Deliv.*, vol. 32, no. 2, pp. 617-627, April 2017.

[20] L. Huang, H. Xin, Z. Wang, L. Zhang, K. Wu and J. Hu, "Transient Stability Analysis and Control Design of Droop-Controlled Voltage Source Converters Considering Current Limitation," *IEEE Trans. Smart Grid*, vol. 10, no. 1, pp. 578-591, Jan. 2019.

[21] K. Ji, G. Tang, H. Pang and J. Yang. "Impedance Modeling and Analysis of MMC-HVDC for Offshore Wind Farm Integration," *IEEE Trans. Power Deliv.*, vol. 35, no. 3, pp. 1488-1501, June 2020,

J. Xu, A. M. Gole and C. Zhao, "The use of averaged-value model of modular multilevel converter in DC grid," *IEEE Trans. Power Deliv.*, vol. 30, no. 2, pp. 519-528, April 2015.

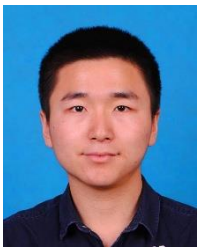

Yingbiao Li received the B.S. degree in electrical engineering from Wuhan University, Wuhan, China, in 2014, the M.S. degree and the Ph.D. degree from China Electric Power Research Institute, Beijing, China, in 2017 and 2020, respectively. He is currently a Postdoctoral Fellow with the State Key Laboratory of Advanced Electromagnetic Engineering and Technology, and School of Electrical and Electronic Engineering, Huazhong University of Science and Technology. His main research interest is transient stability analysis of the power electronic based power systems.

Xiongfei Wang (S'10-M'13-SM'17) received the B.S. degree from Yanshan University, Qinhuangdao, China, in 2006, the M.S. degree from Harbin Institute of Technology, Harbin, China, in 2008, both in electrical engineering, and the Ph.D. degree in energy technology from Aalborg University, Aalborg, Denmark, in 2013.

Since 2009, he has been with the Department of Energy Technology, Aalborg University, where he became an Assistant Professor in 2014, an Associate Professor in 2016, a Professor and Research Program Leader for Electronic Power Grid (eGrid) in 2018, and the Director of Aalborg University-Huawei Energy Innovation Center in 2020. His current research interests include modeling and control of grid-interactive power converters, stability and power quality of converter-based power systems, active and passive filters.

Dr. Wang was selected into Aalborg University Strategic Talent Management Program in 2016. He has received six IEEE Prize Paper Awards, the 2016 Outstanding Reviewer Award of IEEE TRANSACTIONS ON POWER ELECTRONICS, the 2018 IEEE PELS Richard M. Bass Outstanding Young Power Electronics Engineer Award, the 2019 IEEE PELS Sustainable Energy Systems Technical Achievement Award, and the 2019 Highly Cited Researcher by Clarivate Analytics (former Thomson Reuters). He serves as a Member at Large for Administrative Committee of IEEE Power Electronics Society in 2020-2022, and an Associate Editor for the IEEE TRANSACTIONS ON POWER ELECTRONICS, the IEEE TRANSACTIONS ON INDUSTRY APPLICATIONS, and the IEEE JOURNAL OF EMERGING AND SELECTED TOPICS IN POWER ELECTRONICS.

Jianbo Guo received the B.S. degrees from Huazhong University of Science and Technology, Wuhan, China, in 1982 and M.S. degrees from China Electric Power Research Institute, Beijing, China, in 1984.

From 2010 to 2019, he worked as Chairman of China Electric Power Research Institute. Since 2013, he has been an elected Academician of the Chinese Academy of Engineering, Beijing, China. He is currently the deputy chief engineer of State Grid Corporation of China, the vice Chairman of China Electrical Engineering Society, the Honorary Chairman of China Electric Power Research Institute and an adjunct professor with the School of Electrical and Electronic Engineering, Huazhong University of Science and Technology. He has been dedicated to the clean use of energy and the development of environmentally friendly power grid. He has long engaged in power system analysis & control. He has made remarkable achievements in power grid planning, improving security, reliability and transfer capability of power grid, and security of wind power integration. As the principal investigator, he participated in Chinese National Programs for Three Gorges Power Transmission Project and many other important grid planning studies. He presided over the development plan for Chinese National Grid Interconnection Project (from 2020 to 2050). He successfully developed Thyristor Controlled Series Compensation (TCSC) and UHV series compensator (1000kV) with proprietary IPR.

Prof. Guo won the first and second prizes of the National Science and Technology Progress Award in 2008 and 2015, the Ho Leung Ho Lee Foundation Science and Technology Progress Award in 2011 and FEIAP Engineer of the Year Award 2018, in 2019.

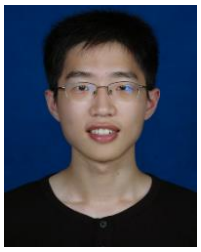

Heng Wu (S'17) received B.S. and M.S. degrees in electrical engineering from Nanjing University of Aeronautics and Astronautics (NUAA), Nanjing, China, in 2012 and 2015, respectively, and the Ph.D. degree in power electronic engineering from Aalborg University, Aalborg, Denmark. He is now a Postdoctoral researcher with the Department of Energy Technology, Aalborg University.

From 2015 to 2017, He was an Electrical Engineer with NR Electric Co., Ltd, Nanjing, China. He was a guest researcher with Ørsted Wind Power, Fredericia, Denmark, from November to December, 2018, and with Bundeswehr University Munich, Germany, from September to December, 2019. His research interests include the modelling and stability analysis of the power electronic based power systems. He received the 2019 Outstanding Reviewer Award of the IEEE TRANSACTIONS ON POWER ELECTRONICS.

Bing Zhao (M'11) received the B.S. and M.S. degrees from Xi'an University of Technology, Xi'an, China, in 2003 and 2006, respectively, both in electrical engineering, and the Ph.D. degree from China Electric Power Research Institute, Beijing, China, in 2009.

Since 2009, he has been with the China Electrical Power Research Institute. He is a senior engineer. His current interests involve the areas of power system analysis and control.

Shanshan Wang received the B.S. and M.S. degrees in electrical engineering from Shandong University, Ji'nan, Chain, in 2003 and 2006, respectively, and the Ph.D. degree from China Electric Power Research Institute, Beijing, China, in 2011.

From 2008 to 2020, as a core member, she participated in the scientific research and engineering solution of Shanghai Nanhui transmission system and Zhangbei ±500kV DC grid based on VSC, devoted to the research of mathematical model, control theory and topology structure on VSC transmission system, and accumulated rich scientific research and engineering experience in this field.

Guanglu Wu received the B.S. degree from North China Electric Power University, Beijing, China, in 2012 and the PhD degree from China Electric Power Research Institute, Beijing, China, in 2018, both in electrical engineering. He is currently working as an engineer in the Power System Department of China Electric Power Research Institute, Beijing, China.

His research interests include VSC-HVDC, DC grid, power converter control and stability analysis of the power system with power electronic devices.

Tiezhu Wang received the B.Eng. degree from Tsinghua University, Beijing, China, in 2012 and the M.S. Degree from China Electric Power Research Institute, Beijing, China, in 2015, both in electrical engineering. He is currently working toward the Ph.D. degree with the Power System Department, China Electric Power Research Institute.

His current research interests include LCC-HVDC, VSC-HVDC, power system simulation, and stability analysis for the power system with high penetrations of power electronics.